

Dielectric backed conducting strips as inductive element in spatial band-pass filter design

Habib GHORBANINEJAD*, Ali GHAJAR

Department of Electrical Engineering, University of Guilan, Rasht, Iran

Received: 12.08.2015

Accepted/Published Online: 18.08.2016

Final Version: 29.05.2017

Abstract: In this paper a new method has been presented to design spatial band-pass filters consisting of dielectric backed conducting strips. This approach uses an equivalent circuit model in which determined inductive elements are spaced at intervals about half wavelength. To realize the proposed method, the inductive elements have been replaced by dielectric backed conducting strips located at intervals about half wavelength. Half wavelength transmission line sections act as resonators. In this manner the wideness and spacing of strips in each dielectric backed conducting strip, as well as the distance between them, is determined by fitting the characteristic (transfer function) of the proposed filter to that of a desired one obtained from an equivalent circuit model. To take the effect of higher order modes (evanescent mode), a coupled set of magnetic field integral equations is derived and formulated. Finally a set of linear matrix equations are solved using method of moments (MoM) and entire basis functions have been used resulting in rapid convergence. The usefulness of the proposed structure and its performance are verified by designing and simulating an equal ripple Chebyshev-type and a Butterworth-type spatial band-pass filter.

Key words: Spatial band-pass filters, frequency selective surfaces, coupled magnetic field integral equations

1. Introduction

Frequency selective surfaces (FSSs) attract a significant amount of interest and they have been investigated in a variety of subjects such as electromagnetic filtering devices for reflector antenna systems, radomes, absorbers, artificial electromagnetic band-gap materials, and spatial microwave and optical filters [1–4]. An FSS is a planar structure that is composed of one or more metallic sheets, each backed by a thin dielectric slab. The overall frequency response of the structure, such as its bandwidth, transfer function, and its dependence on the incident wave angle and polarization, can be determined by the element type and geometry, the substrate parameters, and interelement spacing. To date, different approaches have been used to design FSSs, such as the FSS of antenna-filter-antenna arrays [5], the FSS of aperture coupled micro-strip patches [6], and high selectivity waveguide filters by using genetic algorithm designed FSSs [7]. In [8–10] band-pass filters based on cascading substrate integrated waveguide (SIW) cavities have been designed. In [11] a spatial band-pass filter using FSSs is presented in which each FSS pattern is designed using a genetic algorithm. The developed design method in [11] uses patterned planes as resonating FSSs to realize spatial band-pass filters. In addition, this method can be used to design a desired transfer function using patterned planes in the frequency band. However, a large number of variables should be obtained using the genetic algorithm, which is a time-consuming process and it is complicated to fabricate.

*Correspondence: ghorbaninejad@guilan.ac.ir

In this paper a new method is presented to design spatial band-pass filters. The proposed method uses dielectric backed conducting strips as inductive strips as a simple structure. The values of inductive elements can be obtained using an equivalent circuit model. Instead of a large number of variables, only a few variables are used in the presented method. Dielectric backed conducting strips act as inductive elements located at about half wavelength distances as resonators. In fact, this article is a good extension of [12] to include nonhomogeneous regions to model a resonator. Moreover, the method presented in this article can be modified to include nonhomogeneous regions with a desired number of dielectric slabs that may improve the overall performance of the filter. The characteristics of the proposed filter determine the wideness of strips and their spacing on a dielectric slab. To take the effect of higher order modes (evanescent mode), we apply the coupled set of magnetic field integral equations for the analysis of spatial filters. The derived integral equations are solved by method of moments and using entire basis functions, which results in rapid convergence. Numerical results obtained from the coupled integral equations technique are compared to those from the HFSS software to demonstrate the accuracy of the technique.

2. Coupled integral equation technique

Figure 1 shows the geometry of the proposed spatial band-pass filter consisting of four frequency selective surfaces in the form of dielectric backed conducting strips. This structure is a simple two-dimensional periodic structure, so that metal strips have been glued easily on the dielectric slab. Relative permittivity of dielectric slabs is ϵ_{r1} , ϵ_{r2} , ϵ_{r3} , and ϵ_{r4} with thickness d_1 , d_2 , d_3 , and d_4 , respectively. Figure 2 shows the geometry of the unit cell of the structure and equivalent magnetic currents where g_i is the distance between two strips. Figure 3 shows the equivalent structure for obtaining fields in various regions. The field in the region $0 < z < l_1$ and $l_1 < z < l_1 + l_2$ is only due to induced magnetic current on the aperture parts of diaphragms 1, 2 and diaphragms 2, 3 respectively and so on. In the same way the electric and magnetic field in the region $z > l_1 + l_2 + l_3$ is due to induced magnetic current on the aperture parts of diaphragm 4 only, but the continuity of the magnetic fields across the apertures of diaphragms provides the interaction of all regions that necessitates the formulation of the problem in terms of coupled magnetic integral equations.

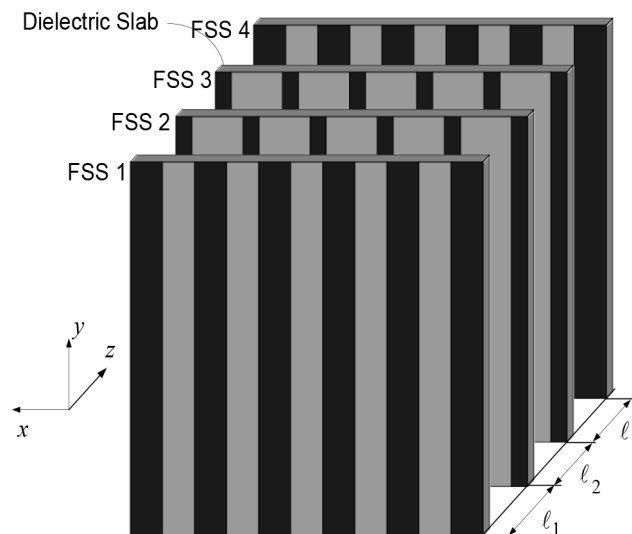


Figure 1. Geometry of proposed spatial band-pass filter consisting of four FSSs in the form of dielectric backed conducting strips.

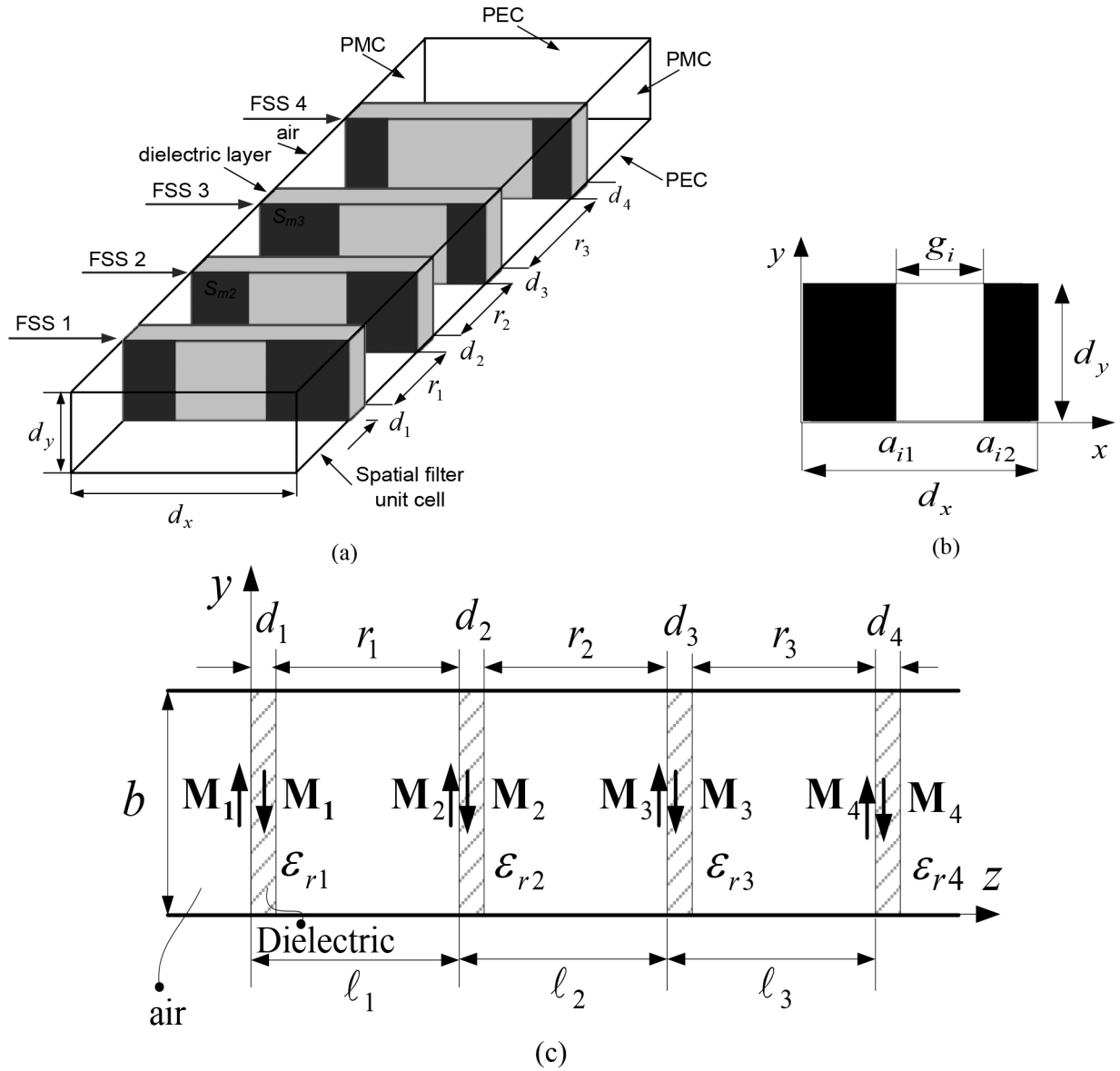


Figure 2. Geometry of a unit cell of a structure consisting of four FSSs in the form of dielectric backed conducting strips. (a) Three-dimension view. (b) Front view of a unit cell of a FSS. (c) Side view and equivalent magnetic currents.

One can derive the appropriate spectral domain Green’s functions for these equivalent structures. The enforcement of continuity of transverse magnetic fields across the aperture parts provides the interaction of all regions. A coupled set of magnetic field integral equations is obtained by enforcing tangential component of magnetic fields on the aperture part of diaphragms.

To derive a typical appropriate spectral Green’s function, one can refer to Figure 4. In this figure $z = 0$, $z = d + r$ are perfect electric conductor and surface magnetic current is assumed to be located on $z = 0^+$. Fourier transforms of tangential components of electric and magnetic fields due to y-directed surface magnetic currents in the region $0 < z < d$ are as follows:

$$\tilde{H}_{x,m} = C_1 k_x Y_d^{TE} \exp(-\gamma dz) - C_2 k_x Y_d^{TE} \exp(\gamma dz) \tag{1}$$

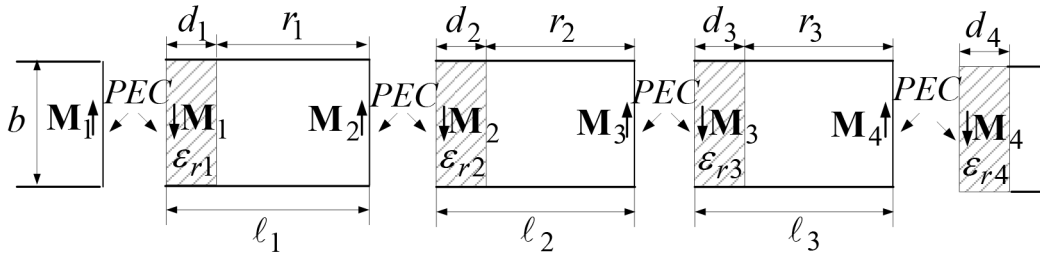


Figure 3. Various regions of equivalent structures for obtaining fields of the structure shown in Figure 1.

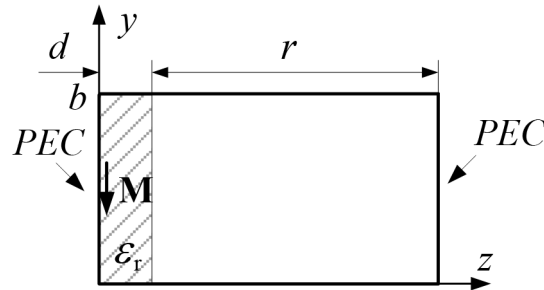


Figure 4. A typical region in Figure 3 to obtain spectral Green's functions in the region $0 < z < d + r$.

$$\tilde{E}_{y,m} = -C_1 k_x \exp(-\gamma_d z) - C_2 k_x \exp(\gamma_d z) \tag{2}$$

Moreover, the above expressions for the electric and magnetic tangential components in the region $d < z < d + r$ are as the following:

$$\tilde{H}_{x,m} = C_3 k_x Y_a^{TE} \exp(-\gamma_a z) - C_4 k_x Y_a^{TE} \exp(\gamma_a z) \tag{3}$$

$$\tilde{E}_{y,m} = -C_3 k_x \exp(-\gamma_a z) - C_4 k_x \exp(\gamma_a z) \tag{4}$$

By applying appropriate boundary conditions (Dirac function has been assumed as magnetic current point source), unknown coefficients C_i are obtained, so that we have:

$$\tilde{H}_x \Big|_{z=0^+} = Y_d^{TE} \frac{Y_a^{TE} + Y_d^{TE} \tanh(\gamma_d d) \tanh(\gamma_a r)}{Y_d^{TE} \tanh(\gamma_a r) + Y_a^{TE} \tanh(\gamma_d d)} \tag{5}$$

The magnetic fields of other parts can be obtained in the same way. All variables of Eqs. (1) to (5) are defined in Appendix A.

In the following, the final expressions for the magnetic fields are given. All appropriate variables are defined in Appendix A; tangential magnetic fields at the diaphragms, approaching from either side of them, take the following forms. Quantities with a tilde (\sim) are Fourier transforms of corresponding quantities without a tilde. The Fourier transform is defined in Appendix A.

$$\tilde{H}_x \Big|_{z=0^-} = Y_m^1 \tilde{M}_1 \tag{6}$$

$$\tilde{H}_x \Big|_{z=0^+} = -Y_m^2 \tilde{M}_1 \tag{7}$$

$$\tilde{H}_x^{sc} \Big|_{z=0^+} = -Y_m^3 \tilde{M}_2 \quad (8)$$

$$\tilde{H}_x \Big|_{z=\ell_1^-} = Y_m^4 \tilde{M}_2 \quad (9)$$

$$\tilde{H}_x^{sc} \Big|_{z=\ell_1^-} = Y_m^5 \tilde{M}_1 \quad (10)$$

$$\tilde{H}_x \Big|_{z=\ell_1^+} = -Y_m^6 \tilde{M}_2 \quad (11)$$

$$\tilde{H}_x^{sc} \Big|_{z=\ell_1^+} = -Y_m^7 \tilde{M}_3 \quad (12)$$

$$\tilde{H}_x \Big|_{z=(\ell_1+\ell_2)^-} = Y_m^8 \tilde{M}_3 \quad (13)$$

$$\tilde{H}_x^{sc} \Big|_{z=(\ell_1+\ell_2)^-} = Y_m^9 \tilde{M}_2 \quad (14)$$

$$\tilde{H}_x \Big|_{z=(\ell_1+\ell_2)^+} = -Y_m^{10} \tilde{M}_3 \quad (15)$$

$$\tilde{H}_x^{sc} \Big|_{z=(\ell_1+\ell_2)^+} = -Y_m^{11} \tilde{M}_4 \quad (16)$$

$$\tilde{H}_x \Big|_{z=(\ell_1+\ell_2+\ell_3)^-} = Y_m^{12} \tilde{M}_4 \quad (17)$$

$$\tilde{H}_x^{sc} \Big|_{z=(\ell_1+\ell_2+\ell_3)^-} = Y_m^{13} \tilde{M}_3 \quad (18)$$

$$\tilde{H}_x \Big|_{z=(\ell_1+\ell_2+\ell_3)^+} = -Y_m^{14} \tilde{M}_4 \quad (19)$$

After enforcing continuity of the tangential magnetic field across the aperture parts of diaphragms in the spatial domain, we obtain:

$$H_{inc,x} + H_x \Big|_{z=0^-} = H_x \Big|_{z=0^+} + H_x^{sc} \Big|_{z=0^+} \quad (20)$$

$$H_x \Big|_{z=\ell_1^-} + H_x^{sc} \Big|_{z=\ell_1^-} = H_x \Big|_{z=\ell_1^+} + H_x^{sc} \Big|_{z=\ell_1^+} \quad (21)$$

$$H_x \Big|_{z=(\ell_1+\ell_2)^-} + H_x^{sc} \Big|_{z=(\ell_1+\ell_2)^-} = \quad (22)$$

$$H_x \Big|_{z=(\ell_1+\ell_2)^+} + H_x^{sc} \Big|_{z=(\ell_1+\ell_2)^+}$$

$$H_x \Big|_{z=(\ell_1+\ell_2+\ell_3)^-} + H_x^{sc} \Big|_{z=(\ell_1+\ell_2+\ell_3)^-} = H_x \Big|_{z=(\ell_1+\ell_2+\ell_3)^+} \quad (23)$$

By expressing the magnetic tangential fields, in term of magnetic currents, the following matrix equations are obtained:

$$\sum_{m=0}^{\infty} [(Y_m^1 + Y_m^2) \phi(x) \int_{ap} \phi(x') M_1(x') dx' + Y_m^3 \phi(x) \int_{ap} \phi(x') M_2(x') dx'] = -H_{inc, x} \quad (24)$$

$$\sum_{m=0}^{\infty} [Y_m^5 \phi(x) \int_{ap} \phi(x') M_1(x') dx' + (Y_m^4 + Y_m^6) \phi(x) \int_{ap} \phi(x') M_2(x') dx' + Y_m^7 \phi(x) \int_{ap} \phi(x') M_3(x') dx'] = 0 \quad (25)$$

$$\sum_{m=0}^{\infty} [Y_m^9 \phi(x) \int_{ap} \phi(x') M_2(x') dx' + (Y_m^8 + Y_m^{10}) \phi(x) \int_{ap} \phi(x') M_3(x') dx' + Y_m^{11} \phi(x) \int_{ap} \phi(x') M_4(x') dx'] = 0 \quad (26)$$

$$\sum_{m=0}^{\infty} [Y_m^{13} \phi(x) \int_{ap} \phi(x') M_3(x') dx' + (Y_m^{12} + Y_m^{14}) \phi(x) \int_{ap} \phi(x') M_4(x') dx'] = 0 \quad (27)$$

where $\phi(x)$ has been defined in Appendix A. To solve these sets of coupled integral equations, we expand magnetic currents in a series of basis functions and then apply Galerkin's method to each one of them. Let $B_j^i(x)$ denote the j -th element of a set of basis functions for the function $M_i(x)$, so we have:

$$M_i(x) = \sum_{j=1}^{N_i} C_{ij} B_j^i(x), i = 1, 2, 3, 4. \quad (28)$$

If these expansion are used in the integral equations and Galerkin's method is applied to each one of them, a set of coupled linear equations results. The three linear equations can be put in the following form:

$$\mathbf{A}_1 \mathbf{C}_1 + \mathbf{A}_2 \mathbf{C}_2 = \mathbf{U}_{inc} \quad (29)$$

$$\mathbf{A}_3 \mathbf{C}_1 + \mathbf{A}_4 \mathbf{C}_2 + \mathbf{A}_5 \mathbf{C}_3 = \mathbf{0} \quad (30)$$

$$\mathbf{A}_6 \mathbf{C}_2 + \mathbf{A}_7 \mathbf{C}_3 + \mathbf{A}_8 \mathbf{C}_4 = \mathbf{0} \quad (31)$$

$$\mathbf{A}_9 \mathbf{C}_3 + \mathbf{A}_{10} \mathbf{C}_4 = \mathbf{0} \quad (32)$$

Matrices in (29) to (32) are given in Appendix B. It is notable that some of these matrices may be equal in symmetrical conditions, a fact that is used to reduce the computational effort. It is worth noting that (29) to

(32) follow a clear pattern, which allows the number of dielectric backed conducting strips to be varied relatively simply. Here according to the conditions of the structure the following basis functions are given [12]:

$$M_i(x) = \sum_{j=1}^{N_i} C_{ij} B_j^i(x) = \sum_{j=1}^{N_i} C_{ij} \frac{\sin[j\pi(x-a_{i1})/g_i]}{[(x-a_{i1})(g_i+a_{i1}-x)]^{1/3}}, \quad i = 1, 2, 3, 4. \quad (33)$$

The spectra of these basis functions are expressible in terms of Bessel functions of the first kind of order 1/6 and have been given in Appendix B.

3. Design procedure

A band-pass filter consisting of N series resonators and $N + 1$ impedance invertors has been considered. The value of impedance invertors and the elements of resonators can be obtained according to the type of filter transfer function, center frequency, and the bandwidth of the filter. This circuit model can be realized by $N + 1$ shunt inductances and N transmission line sections. Figure 5 shows the circuit model approach of such a typical filter, which is composed of inductive elements that are located in the intervals of half wavelength transmission lines. Diaphragms in Figure 2 act as inductances and distances between them act as resonators. The main problem is to design dielectric backed conducting strips to act as shunt elements. In the design process aperture widths of diaphragms and the distances between them are optimized so that the transmission characteristic of the filter can be fitted to that of the circuit model. The fitness function is given by

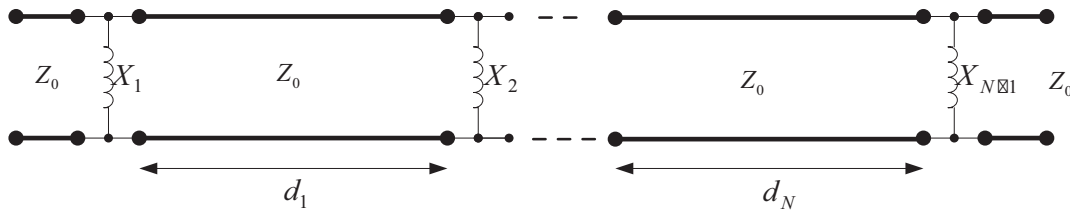


Figure 5. Circuit model approach of a typical band-pass filter.

$$\text{fitness} = \frac{1}{N_S + N_P} \left\{ \sum_{i=1}^{N_S} |S_{21}^{CIET}(f_i) - S_{21}^{LC}(f_i)|^2 + \sum_{i=1}^{N_P} |S_{21}^{CIET}(f_i) - S_{21}^{LC}(f_i)|^2 \right\}^{0.5} \quad (34)$$

In (34) $S_{21}^{CIET}(f_i)$ and $S_{21}^{LC}(f_i)$ are the S-parameters of the coupled integral equation technique model and circuit model approach, respectively, which are evaluated in frequency sample f_i . N_P and N_S are the number of frequency samples in the pass-band and each of the stop bands, respectively. The optimization process can be performed using arbitrary initial values to obtain the lengths of transmission line sections and the aperture widths of diaphragm.

4. Design examples and results

Example 1 *Chebyshev-type spatial band-pass filter.* In the first example, a 3-order Chebyshev-type spatial band-pass filter with center frequency $f_0 = 10$ GHz, relative bandwidth of 10%, and equal ripples of 0.5 has been designed. The dimensions of the unit cell $d_x = 20$ mm and $d_y = 10$ mm are considered. This filter is made of four dielectric backed conducting strips as inductances, which are supported by small thickness dielectric slabs, $d_1 = d_2 = d_3 = d_4 = 0.4$ mm, and relative electric permittivity of $\epsilon_{r1} = \epsilon_{r2} = \epsilon_{r3} = \epsilon_{r4} = 3.8$. The designed values of aperture widths and distances between them are given in the following Table. Figure 6 shows the transmission characteristics of the designed filter and the simulated one. The LC prototype transmission characteristics obtained from the equivalent circuit model are shown in the figure. Comparison between the calculated and simulated results shows good agreement over the frequency range. In the design example, the thickness of dielectric slabs and their electric permittivity have been chosen from existing commercial types. The code has been written in MATLAB and an Intel Pentium CPU G3240@3.1 GHz 4 GB RAM computer has been used. This leads to a computation time of 10 s to calculate the transmission coefficient of the structure, while the same time for the design method presented in [11] is about 25 min. Since in the presented model all the parameters have been taken into account, there is no limitation in utilizing common existing dielectric slabs.

Table. The physical parameters of designed band-pass filters.

Lengths and widths [mm]	Designed values	
	Chebyshev type	Butterworth type
a	20	20
b	10	10
$g_1 = g_4$	9.8317	10.9
$g_2 = g_3$	6.2691	5.6
$r_1 = r_3$	12.687	12.49
r_2	13.5851	13.79

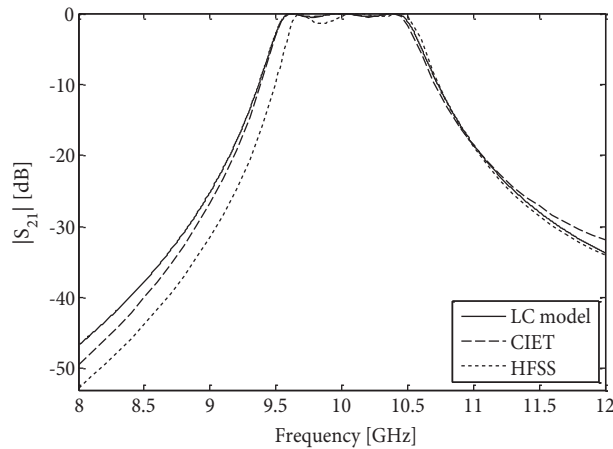


Figure 6. Transmission characteristic of Chebyshev-type spatial band-pass filter.

Example 2 *Butterworth-type spatial band-pass filter.* In the second example, a 2-order Chebyshev-type spatial band-pass filter with center frequency $f_0 = 10$ GHz and relative bandwidth of 9% has been designed. The

dimensions of the unit cell, and thickness and relative permittivity of the dielectric slabs are the same as in example one. The designed values of aperture widths and distances between them are given in the Table. Figure 7 shows the transmission characteristics of the designed Butterworth-type spatial band-pass filter and the simulated one. Calculated and simulated results are in good agreement over the frequency range. In both examples, symmetrical condition has been considered.

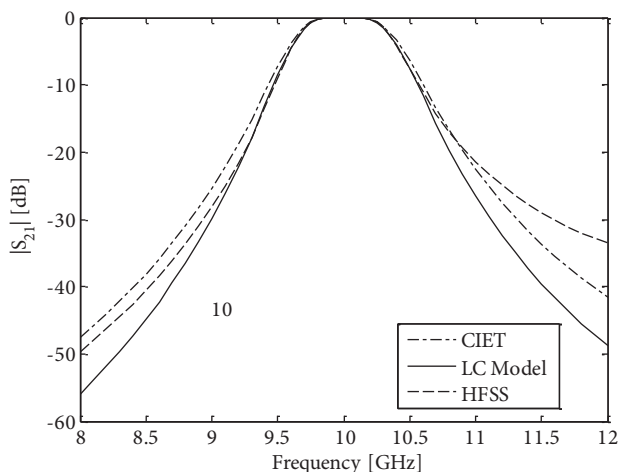


Figure 7. Transmission characteristic of Butterworth-type spatial band-pass filter.

5. Conclusion

In this paper a new method has been proposed to design a spatial band-pass filter consisting of dielectric backed conducting strips. The design process of such filters is basically based on an equivalent circuit approach in which inductive elements are located in the intervals of about half wavelength, so that conducting strips on each slab act as an appropriate inductive element. In accordance with the proposed structure, derived magnetic fields integral equations have been solved using an entire domain basis function. In the proposed structure, a few design parameters (optimization parameters), which are the wideness of strips and strip's distances, have been optimized. Therefore, design parameters can be obtained easily using a fast optimization according to the defined entire domain basis function. At the expense of larger longitudinal length, the new proposed structure can be fabricated easily because they have been made of conducting strips glued on a dielectric slab. The proposed method can be applied to design Chebyshev and Butterworth band-pass filters. The numerical and simulated verification shows the usefulness of the proposed spatial band-pass filter.

References

- [1] Munk BA. Frequency Selective Surfaces: Theory and Design. Hoboken, NJ, USA: Wiley, 2000.
- [2] Kern DJ, Werner DH. A genetic algorithm approach to the design of ultra-thin electromagnetic band-gap absorbers. *Microw Opt Techn Let* 2003; 38: 61-64.
- [3] Kern DJ, Werner DH, Wilhelm MJ. Genetically engineered multi-band high impedance frequency selective surfaces. *Microw Opt Techn Let* 2003; 38: 400-403.
- [4] Chen C. Scattering by a two-dimensional periodic array of ducting plates. *IEEE T Antenn Propag* 1970; 18: 660-665.
- [5] Abbaspour A, Sarabandi K, Rebeiz GM. Antenna-filter-antenna arrays as a class of bandpass-frequency selective surfaces. *IEEE T Microw Theory* 2004; 52: 1781-1789.

- [6] Pous R, Pozar DM. A frequency-selective surface using aperture coupled micro-strip patches. *IEEE T Antenn Propag* 1991; 39: 1763-1769.
- [7] Ohira M, Deguchi H, Tsuji M, Shigesawa H. Multi band single layer frequency selective surface designed by combination of genetic algorithm and geometry-refinement technique. *IEEE T Microw Theory* 2004; 52: 2925-2931.
- [8] Zhang YL, Hong W, Wu K, Chen JX, Tang HJ. Novel substrate integrated waveguide cavity filter with defected ground structure. *IEEE T Microw Theory* 2005; 53: 1280-1287.
- [9] Hao ZC, Hong W, Chen JX, Chen XP, Wu K. Compact super wide band pass substrate integrated waveguide filters. *IEEE T Microw Theory* 2005; 53: 2968-2977.
- [10] Luo GQ, Hong W, Tang HJ, Wu K. High performance frequency selective surface using cascading substrate integrated waveguide cavities. *IEEE Microw Wirel Co* 2006; 16: 648-650.
- [11] Ghorbaninejad H, Khalaj-Amirhosseini M. Compact spatial band-pass filters using frequency selective surfaces. *Prog Electromagn Res B* 2011; 21: 59-73.
- [12] Ghorbaninejad H, Khalaj-Amirhosseini M. Compact band pass filters utilizing dielectric filled waveguides. *Prog Electromagn Res B* 2008; 7: 105-115.

A. Appendix

Quantities with a tilde (\sim) are Fourier transforms of corresponding quantities without a tilde.

$$Y_m^1 = Y_a^{TE} \quad (\text{A.1})$$

$$Y_m^2 = Y_{d1}^{TE} \frac{Y_a^{TE} + Y_{d1}^{TE} \tanh(\gamma_{d1} d_1) \tanh(\gamma_a r_1)}{Y_{d1}^{TE} \tanh(\gamma_a r_1) + Y_a^{TE} \tanh(\gamma_{d1} d_1)} \quad (\text{A.2})$$

$$Y_m^3 = Y_a^{TE} Y_{d1}^{TE} \frac{1}{\cosh(\gamma_{d1} d_1) \cosh(\gamma_a r_1)} \cdot \frac{1}{Y_{d1}^{TE} \tanh(\gamma_a r_1) + Y_a^{TE} \tanh(\gamma_{d1} d_1)} \quad (\text{A.3})$$

$$Y_m^4 = Y_a^{TE} \frac{Y_{d1}^{TE} + Y_a^{TE} \tanh(\gamma_{d1} d_1) \tanh(\gamma_a r_1)}{Y_a^{TE} \tanh(\gamma_{d1} d_1) + Y_{d1}^{TE} \tanh(\gamma_a r_1)} \quad (\text{A.4})$$

$$Y_m^5 = Y_m^3 \quad (\text{A.5})$$

$$Y_m^6 = Y_{d2}^{TE} \frac{Y_a^{TE} + Y_{d2}^{TE} \tanh(\gamma_{d2} d_2) \tanh(\gamma_a r_2)}{Y_{d2}^{TE} \tanh(\gamma_a r_2) + Y_a^{TE} \tanh(\gamma_{d2} d_2)} \quad (\text{A.6})$$

$$Y_m^7 = Y_a^{TE} Y_{d2}^{TE} \frac{1}{\cosh(\gamma_{d2} d_2) \cosh(\gamma_a r_2)} \cdot \frac{1}{Y_{d2}^{TE} \tanh(\gamma_a r_2) + Y_a^{TE} \tanh(\gamma_{d2} d_2)} \quad (\text{A.7})$$

$$Y_m^8 = Y_a^{TE} \frac{Y_{d2}^{TE} + Y_a^{TE} \tanh(\gamma_{d2} d_2) \tanh(\gamma_a r_2)}{Y_a^{TE} \tanh(\gamma_{d2} d_2) + Y_{d2}^{TE} \tanh(\gamma_a r_2)} \quad (\text{A.8})$$

$$Y_m^9 = Y_m^7 \quad (\text{A.9})$$

$$Y_m^{10} = Y_{d3}^{TE} \frac{Y_a^{TE} + Y_{d3}^{TE} \tanh(\gamma_{d3} d_3) \tanh(\gamma_a r_3)}{Y_{d3}^{TE} \tanh(\gamma_a r_3) + Y_a^{TE} \tanh(\gamma_{d3} d_3)} \quad (\text{A.10})$$

$$Y_m^{11} = Y_a^{TE} Y_{d3}^{TE} \frac{1}{\cosh(\gamma_{d3} d_3) \cosh(\gamma_a r_3)} \cdot \frac{1}{Y_{d3}^{TE} \tanh(\gamma_a r_3) + Y_a^{TE} \tanh(\gamma_{d3} d_3)} \quad (\text{A.11})$$

$$Y_m^{12} = Y_a^{TE} \frac{Y_{d3}^{TE} + Y_a^{TE} \tanh(\gamma_{d3} d_3) \tanh(\gamma_a r_3)}{Y_a^{TE} \tanh(\gamma_{d3} d_3) + Y_{d3}^{TE} \tanh(\gamma_a r_3)} \quad (\text{A.12})$$

$$Y_m^{13} = Y_m^{11} \quad (\text{A.13})$$

$$Y_m^{14} = Y_{d4}^{TE} \frac{Y_a^{TE} + Y_{d4}^{TE} \tanh(\gamma_{d4} d_4)}{Y_{d4}^{TE} + Y_a^{TE} \tanh(\gamma_{d4} d_4)}, \quad (\text{A.14})$$

where

$$Y_{di}^{TE} = \frac{\gamma_{di}}{j\omega\mu_0}, \quad i = 1, 2, 3, 4. \quad (\text{A.15})$$

$$Y_a^{TE} = \frac{\gamma_a}{j\omega\mu_0} \quad (\text{A.16})$$

$$\gamma_a = \sqrt{k_x^2 - \omega^2\mu_0\varepsilon_0} \quad (\text{A.17})$$

$$\gamma_{di} = \sqrt{k_x^2 - \omega^2\mu_0\varepsilon_0\varepsilon_{ri}}, \quad i = 1, 2, 3, 4. \quad (\text{A.18})$$

$$k_x = 2m\pi/a \quad (\text{A.19})$$

$$\tilde{f}(k_x) = \int_{x=0}^a f(x) \phi(x) dx \quad (\text{A.20})$$

$$f(x) = \int_{x=0}^a \tilde{f}(x) \phi(x) dk_x \quad (\text{A.21})$$

$$\phi(x) = (\varepsilon_{0m}/a)^{0.5} \cos(k_x x) \quad (\text{A.22})$$

$$\varepsilon_{0m} = \begin{cases} 1 & , m = 0 \\ 2 & , m \neq 0 \end{cases} \quad (\text{A.23})$$

B. Appendix

\tilde{B}_k^i are the Fourier transform of basis functions.

$$[\mathbf{A}_1]_{k\ell} = \sum_{m=0}^{\infty} \tilde{B}_k^1 (Y_m^1 + Y_m^2) \tilde{B}_\ell^1 \quad (\text{B.1})$$

$$[\mathbf{A}_2]_{k\ell} = \sum_{m=0}^{\infty} \tilde{B}_k^1 Y_m^3 \tilde{B}_\ell^2 \quad (\text{B.2})$$

$$[\mathbf{A}_3]_{k\ell} = \sum_{m=0}^{\infty} \tilde{B}_k^2 Y_m^5 \tilde{B}_\ell^1 \quad (\text{B.3})$$

$$[\mathbf{A}_4]_{k\ell} = \sum_{m=0}^{\infty} \tilde{B}_k^2 (Y_m^4 + Y_m^6) \tilde{B}_\ell^2 \quad (\text{B.4})$$

$$[\mathbf{A}_5]_{k\ell} = \sum_{m=0}^{\infty} \tilde{B}_k^2 Y_m^7 \tilde{B}_\ell^3 \quad (\text{B.5})$$

$$[\mathbf{A}_6]_{k\ell} = \sum_{m=0}^{\infty} \tilde{B}_k^3 Y_m^9 \tilde{B}_\ell^2 \quad (\text{B.6})$$

$$[\mathbf{A}_7]_{k\ell} = \sum_{m=0}^{\infty} \tilde{B}_k^3 (Y_m^8 + Y_m^9) \tilde{B}_\ell^3 \quad (\text{B.7})$$

$$[\mathbf{A}_8]_{k\ell} = \sum_{m=0}^{\infty} \tilde{B}_k^3 Y_m^{11} \tilde{B}_\ell^4 \quad (\text{B.8})$$

$$[\mathbf{A}_9]_{k\ell} = \sum_{m=0}^{\infty} \tilde{B}_k^4 Y_m^{13} \tilde{B}_\ell^3 \quad (\text{B.9})$$

$$[\mathbf{A}_{10}]_{k\ell} = \sum_{m=0}^{\infty} \tilde{B}_k^4 (Y_m^{12} + Y_m^{14}) \tilde{B}_\ell^4 \quad (\text{B.10})$$

$$\mathbf{C}_i = \begin{bmatrix} C_{i1} & C_{i2} & \dots & C_{i, N_i} \end{bmatrix}^T, \quad (\text{B.11})$$

$i = 1, 2, 3, 4$

$$[\mathbf{U}_{inc}]_k = 2 Y_a^{TE} \Big|_{m=0} (1/a)^{-0.5} \tilde{B}_k^1 \quad (\text{B.12})$$

$$\begin{aligned} \tilde{B}_j^i &= (2a/\varepsilon_{0m})^{-1/2} g_i^{1/3} \Gamma(0.5) \Gamma(2/3) \\ &\left\{ \frac{1}{|(k_x g_i + \pi j)|^{1/6}} \cdot J_{1/6}(|0.5(k_x g_i + \pi j)|) \cdot \right. \\ &\sin(0.5(k_x g_i + \pi j) + k_x a_{i1}) \\ &- \frac{1}{(k_x g_i - \pi j)^{1/6}} J_{1/6}(0.5(k_x g_i - \pi j)) \\ &\left. \sin(0.5(k_x g_i - \pi j) + k_x a_{i1}) \right\} \\ &\text{if } k_x g_i - \pi j \neq 0 \end{aligned} \quad (\text{B.13})$$

$$\begin{aligned} \tilde{B}_j^i(k_x) &= (2a/\varepsilon_{0m})^{-1/2} g_i^{1/3} \Gamma(0.5) \Gamma(2/3) \\ &\left\{ \frac{(-1)^j}{(2\pi j)^{1/6}} J_{1/6}(\pi j) - \frac{\Gamma(2/3)}{\Gamma(0.5)\Gamma(4/3)} \right\} \sin(k_x a_{i1}) \\ &\text{if } k_x g_i - \pi j = 0 \end{aligned} \quad (\text{B.14})$$